JMEPEG (2024) 33:5195–5205
https://doi.org/10.1007/s11665-023-08360-z

©ASM International
1059-9495/$19.00

TECHNICAL ARTICLE

Preparation and Characterization Studies of Biomass-Based Adsorbents for CO_2 Capture

R. Maniarasu, Sushil Kumar Rathore, and S. Murugan

Submitted: 1 February 2023 / Revised: 2 May 2023 / Accepted: 11 May 2023 / Published online: 6 June 2023

This research work focuses on the preparation and characterization of activated carbons derived from biomass residues as potential adsorbents for carbon dioxide (CO_2) capture applications under ambient conditions. Three abundantly available and inexpensive raw materials, viz., (i) corn cob, (ii) sugarcane bagasse, and (iii) wheat straw, are used to prepare activated carbon using carbonization and activation methods. Characterization techniques such as (a) Nitrogen (N_2) adsorption/desorption, (b) Scanning Electron Microscopy, (c) Fourier Transform Infrared Spectra, (d) Thermogravimetric Analysis, and (e) proximate and ultimate analyses are used to examine the surface texture and physiochemical parameters of the adsorbents, including surface area, pore volume, pore diameter, surface morphology, structural features, thermal stability, and quantitative and elemental compounds. The adsorption–desorption isotherms of CO_2 uptake capabilities of adsorbents are evaluated at 1 bar pressure, with temperatures varying from 0 to 90 °C. The significant parameters of adsorbents' adsorption, such as (i) CO_2 adsorption–desorption isotherms, (ii) CO_2/N_2 adsorption, (iii) recyclability, (iv) breakthrough curve and (v) isosteric heat of adsorption ($\triangle H_{ads}$) are determined. The N_2 adsorption/desorption investigation shows that the tested adsorbents are highly porous and crucial for post-combustion carbon capture. Values of $\triangle H_{ads}$ for activated carbon samples are below 40 kJ/mol, which ensures the physical adsorption process. The findings suggest that adsorbents are most appropriate for multiple gas sorption applications. The anticipated characteristics will benefit for actual system development.

Keywords activated carbon, adsorbent, adsorption isotherms, carbon capture, carbon dioxide, CO_2 adsorption, CO_2 uptake, physical adsorption

1. Introduction

The sudden growth in advanced technology in the twenty-first century has expanded the utilization of fossil fuel energy sources to satisfy energy requirements, which causes emissions of greenhouse gases (GHGs) that impact our ecosystem. These GHGs impact the lifecycle and habits of terrestrial, aquatic, and other living organisms (Ref 1, 2). The main component of anthropogenic GHGs is the carbon dioxide (CO_2) emissions directly released into our environment. It is caused mainly by excessive fossil fuel combustion. The World Meteorological Organization (WMO) and Intergovernmental Panel on Climate Change (IPCC) documented that the 400 ppm CO_2 threshold has already been surpassed and will probably hit 580 ppm within 2100, resulting in the highest CO_2 emissions peaks. This new shift in CO_2 emissions is significantly responsible for global warming potential (GWP) and climate change. These emissions have resulted in the implementation of innovative approaches such as (a) Carbon Capture and Utilization (CCU) and (b) Carbon Capture and Storage (CCS) to achieve net-zero emissions worldwide. CCS is one of the most feasible options as it can capture CO_2 from CO_2 emitting sources and mitigate CO_2 emissions by about 80-95%. There are three distinct CCS strategies: (i) oxy-fuel combustion carbon capture, (ii) post-combustion carbon capture, and (iii) pre-combustion carbon capture (Ref 3, 4). Among all those mentioned CO_2 capture options, post-combustion carbon capture is the most popular approach to capturing CO_2 emissions from fossil fuel combustion (Ref 5).

Appropriate adsorbent choice is essential in the CCS method, particularly in the post-combustion adsorption-based CO_2 capture process. Solid sorbent materials have recently received significant interest as promising CCS options, primarily activated carbon materials. The main merits of activated carbons are (a) inexpensive, (b) superior surface functional groups, (c) large specific surface area, (d) greater pore volume, (e) stability toward moisture, (f) good heat resistance, (g) excellent renewability, (h) superior mechanical and chemical strength, (i) good surface affinity, (j) excellent CO_2 selectivity,

This article is an invited submission to the *Journal of Materials Engineering and Performance* selected from presentations at the 4th International Conference on Processing andCharacterization of Materials (ICPCM 2022) held December 9–11, 2022, at the National Institute of Technology, Rourkela, Odisha, India. It has been expanded from the original presentation. The issue was organized by Prof. Joao Pedro Oliveira, Universidade NOVA de Lisboa, Portugal; Prof. B. Venkata Manoj Kumar, Indian Institute of Technology Roorkee, India; Dr. D. Arvindha Babu, DMRL, DRDO, Hyderabad, India; Prof. Kumud Kant Mehta and Prof. Anshuman Patra, National Institute of Technology Rourkela, Odisha, India; and Prof. Manab Mallik, National Institute of Technology Durgapur, India.

R. Maniarasu, Sushil Kumar Rathore, and **S. Murugan**, Department of Mechanical Engineering, National Institute of Technology Rourkela, Rourkela 769008, Odisha, India. Contact e-mails: maniarasu664@gmail.com and 518me10127@nitrkl.ac.in.

(k) faster kinetics, and (l) tunable porous structure. Due to their numerous inherent advantages in attractive physicochemical properties and excellent surface textural characteristics, activated carbons are used as potential candidates in multiple applications, viz., pharmaceutical, petrochemical, food/beverage, environmental remediation, greenhouse gas capture, automotive, energy storage, and chemical sectors (Ref 6).

Several studies have been conducted on preparing and characterizing biomass-based adsorbents for CO_2 physisorption under ambient conditions. Maniarasu et al. (Ref 7) assessed the CO_2 capture efficiency of adsorbents derived from palm shells using carbonization and potassium hydroxide (KOH) activation. It is reported that a palm shell-based adsorbent shows a surface area of 1450.8 m^2/g and a pore volume of 0.75 cm^3/g. Furthermore, the adsorbent exhibits a maximum CO_2 adsorption isotherm of 4.0 mmol/g at a temperature of 50 °C and pressure of 1 bar. Ding et al. (Ref 8) reported seaweed-activated carbon produced from Sargassum and Enteromorpha. At 1 bar and 25 °C, the maximum CO_2 adsorption capacity of 1.05 mmol/g and 0.52 mmol/g is achieved for Sargassum-activated carbon and Enteromorpha-activated carbon, respectively. The same research group developed activated carbon derived from Pomegranate and Carrot peels using KOH. It is identified that the maximum CO_2 adsorption capacities of 4.11 mmol/g at 1 bar, 25 °C, and 6.033 mmol/g at 1 bar, 0 °C for Pomegranate peel-based activated carbon; and 4.18 mmol/g at 1 bar, 25 °C, and 5.04 mmol/g at 1 bar, 0 °C for Carrot peel-based activated carbon. Ismail et al. (Ref 9) evaluated bamboo-based activated carbon's potential for CO_2 capture. Activated carbon is produced using single-stage activation with different impregnation ratios of phosphoric acid (H_3PO_4). It is found that activated carbon exhibits surface area, pore volume, and average pore size. These values range from 1063-1492 m^2/g, 0.93-1.19 cm^3/g, to 2.49-4.48 nm, respectively. Moreover, 50 wt.% impregnated activated carbon exhibits a maximum CO_2 adsorption capacity of 1.45 mmol/g at 1 bar pressure and 0 °C.

Wu et al. (Ref 10) examined Lotus stem waste-based activated carbon using hydrothermal carbonization followed by KOH and sulfuric acid. The distinct impregnation ratios (1:2 and 1:4) are used to evaluate activated carbon's surface area and porous volume. It is reported that activated carbon exhibits a surface area of 2893 m^2/g and a pore volume of 1.59 cm^3/g at an impregnation ratio of 1:4. Similarly, at the impregnation ratio of 1:2, the same activated carbon shows a maximum CO_2 uptake of 3.85 mmol/g at 1 bar, 25 °C; and 6.17 mmol/g at 1 bar, 0 °C. Maniarasu et al. (Ref 11) evaluated the CO_2 adsorption performance of activated carbon obtained from coconut shells using single-step activation. KOH is used as a chemical activator to improve the surface area and porosity of the developed coconut shell-based activated carbon. It is found that coconut shell-based activated carbon exhibits a surface area of 1248.5 m^2/g and a pore volume of 0.79 cm^3/g. Moreover, the activated carbon shows a maximum CO_2 uptake of 4.6 mmol/g at a temperature of 50 °C and pressure of 1 bar. Gautam et al. (Ref 12) experimentally investigated activated carbons' CO_2 adsorption capacity. In addition, the produced activated carbons are characterized to determine their surface textural characteristics and physicochemical properties. It is reported that activated carbons exhibit surface area, pore volume, and average pore size, ranging from 923-1254 m^2/g, 0.29-0.41 cm^3/g, and 16.78-19.21 Å, respectively. Further, CARB 6X12 55 activated carbon exhibits a maximum CO_2 uptake of 4.53 mmol/g, whereas Norit RB 4 activated carbon shows a minimum CO_2 uptake of 3.02 mmol/g at 1 bar pressure and 0 °C.

Huang et al. (Ref 13) examined the performance of developed N-doped porous enriched CO_2 adsorbents using a two-step synthetic approach. They used three impregnation ratios with three activation temperatures for the activated carbon preparation. It is identified that an optimum impregnation ratio and activation temperature of activated carbon enhances the porous textural characteristics and CO_2 uptake performance of adsorbent samples. Changdan Ma et al. (Ref 14) studied the assessment of N/S-doped carbon material for CO_2 adsorption and supercapacitor. Activated carbon is derived from water chestnut shells using the KOH-chemical activation method. Three activation temperatures and three impregnation ratios are adopted during the process. It is determined that the optimal activation temperature and impregnation ratio of activated carbon exhibits excellent surface textural properties and surface functional groups. Tingyan Lu et al. (Ref 15) evaluated porous carbon for CO_2 adsorption applications. They prepared activated carbon from bitartrate using KOH activation and impregnation ratios. It is found that the optimum activation temperature and impregnation ratio of developed carbon show morphological, structural characteristics, and surface chemical properties. Based on the literature survey, it is observed that the optimum impregnation ratio and suitable activation temperature ensure the surface textural features, physicochemical properties, and maximum CO_2 uptake for adsorption.

In this present study, biomass residues, such as (a) corn cob, (b) sugarcane bagasse, and (c) wheat straw, are selected as suitable raw materials for activated carbon production. They possess the following benefits (a) abundantly available, (b) inexpensive, (c) non-harmful to nature, and (d) easy to handle and modify their properties. A single-stage KOH activation (i.e., carbonization and activation) method is used in this investigation for activated carbon production. Surface textural characteristics and physicochemical properties of produced activated carbons are determined using different analytical and characterization techniques. After ensuring CO_2 capture suitability, the corn cob-, sugarcane bagasse-, and wheat straw-activated carbons are named as corn cob, sugarcane bagasse, and wheat straw adsorbents.

Moreover, the adsorption of CO_2 onto the surface of adsorbent samples is evaluated through adsorption isotherms at various operating conditions. This revealed the surface phenomena (i.e., gas–solid interactions) in the physical adsorption process. This current investigation also highlights CO_2 physical adsorption onto biomass-based adsorbent surfaces. Therefore, this research aims to use eco-friendly and cost-effective activated carbons for carbon capture obtained from renewable biomass resources. The developed porous activated carbon samples exhibit outstanding CO_2 uptake and superior recycling performance over multiple test cycles.

2. Materials, Methods, and Experimental Section

2.1 Sample Selection and Activated Carbon Preparation

2.1.1 Selection of Feedstocks. In this work, biomass substances, such as (i) corn cob, (ii) sugarcane bagasse, and (iii) wheat straw, are procured from the most available areas in

different geographical locations in India. The obtained samples are cleaned with distilled water (H_2O) to remove unwanted substances. They are dried in open sunlight for nearly four weeks. The samples are pre-screened to remove impurities and uneven surface particles. The samples are kept in an oven heated at 150 °C to remove moisture content. After that, the samples are stored in an airtight container before the production process.

2.2 Activated Carbon Preparation

A single-stage activation method is used in the current study to enhance the activated carbon samples' surface textural properties and physicochemical characteristics. Single-stage activation is the combination of carbonization and chemical activation processes. Initially, the samples are soaked in KOH solution at an impregnation ratio of 1:4. The impregnated samples are carbonized. Carbonization is the thermal decomposition in which samples are heated at an activation temperature of 600 °C, a heating rate of 10 °C/min, and a holding time of 1 h in a furnace without oxygen (O_2). During this process, non-carbon elements such as nitrogen (N_2), oxygen (O_2), sulfur (S), and hydrogen (H_2) are removed from samples. The obtained end-products are known as biochar. They possess minimal surface area and porosity on their surfaces. Therefore, the products obtained through carbonization are further washed with hydrochloric acid (HCL) and distilled H_2O to remove unwanted impurities and chemical compounds from their surface. Washing improves final products' pores and surface area. The derived activated carbon samples are further dried at 150 °C overnight. Activated carbon samples are kept in an airtight container before adsorption analysis.

The yield of activated carbon samples is calculated by using Eq. 1 (Ref 16, 17)

$$(\%yield) = \left(\frac{(\text{mass}(g) \text{ of activated carbon})}{(\text{mass}(g) \text{ of sample})}\right) * 100 \qquad \text{(Eq 1)}$$

The result of the activated carbon yield obtained from biomass is presented in Table 1.

2.3 Experimental Section: Characterization of Activated Carbons

The quantitative and elemental compositions of raw materials and activated carbons are obtained using proximate and ultimate analyzers, respectively. The surface textural characteristics and physicochemical properties, viz., specific surface area, pore volume, pore width, and pore size distributions of the activated carbon samples, are characterized using the N_2 sorption isotherm technique. Surface morphological and structural features of activated carbon samples are investigated using SEM. The surface chemical groups of activated carbon samples are analyzed through FTIR. The thermal stability of activated carbons is determined using a TGA analyzer.

3. Results and Discussion

3.1 Proximate and Ultimate Analyses

3.1.1 Proximate Analysis. Proximate analysis is mainly used to determine the percentage of ash content, volatile matter, moisture content, and fixed carbon content in raw materials and activated carbon samples (Ref 7). Table 2 presents the quantitative components of raw materials and activated carbon samples.

It can be observed from the table that quantitative analysis of raw materials and activated carbon samples. The fixed carbon of activated carbon samples is increased by about 30.03, 37.86, and 37.59%, respectively, for sugarcane bagasse-, wheat straw-, and corn cob-activated carbons. Similarly, the other components, such as volatile matter, moisture, and ash contents, are decreased on activated carbon samples during activated carbon preparation. Fixed carbon can strongly interact with adsorbate molecules and adsorbent materials (Ref 18, 19).

3.1.2 Ultimate Analysis. Ultimate analysis is mainly used to examine the percentage of carbon (C), hydrogen (H), nitrogen (N), oxygen (O), and sulfur (S) in raw materials and activated carbon samples (Ref 11). Table 3 provides the elemental compositions of raw materials and activated carbon samples.

It can be inferred from the table that the elemental compositions of raw materials and activated carbon samples. The carbon element of activated carbon samples is increased by about 30.24, 27.22, and 29.78%, respectively, for sugarcane bagasse-, wheat straw-, and corn cob-activated carbons. On the other hand, the remaining elemental compositions, such as H, N, O, and S, are decreased on activated carbon samples during the thermal decomposition process. Carbon element may play a vital role in adsorption performance (Ref 18, 19).

3.2 N_2 Adsorption/Desorption Analysis

In this surface characterization, activated carbon samples' surface textural characteristics, viz., (a) surface area, (b) pore volume, and (c) pore size distribution, are investigated using N_2 adsorption/desorption (Ref 6, 11). These parameters significantly enhance the adsorption performance of activated carbon

Table 1 Percentage of activated carbon yield

Parameter	Sugarcane bagasse-activated carbon	Wheat straw-activated carbon	Corn cob-activated carbon
Amount of biomass, g	120	120	120
Amount of carbon char used in KOH activation, g	98.45	96.67	90.89
Amount of activated carbon produced, g	70.98	68.90	60.75
Yield, %	59.15	57.42	50.63

Table 2 Quantitative components of raw materials and activated carbon samples

Sample examined	Proximate analysis, wt.%			
	Ash content	Volatile matter	Moisture content	Fixed carbon
Sugarcane bagasse	1.94	36.64	5.78	55.64
Sugarcane bagasse-activated carbon	0.98	12.04	1.34	85.67
Wheat straw	3.45	42.98	6.45	47.12
Wheat straw-activated carbon	1.96	10.65	2.41	84.98
Corn cob	4.89	40.87	4.56	49.66
Corn cob-activated carbon	1.25	9.63	1.87	87.25

Table 3 Elemental components of raw materials and activated carbon samples

Sample examined	Ultimate analysis, wt.%				
	C	H	N	O	S
Sugarcane bagasse	56.72	8.99	12.67	20.39	1.23
Sugarcane bagasse-activated carbon	86.96	1.56	4.85	5.46	.99
Wheat straw	55.65	10.45	7.38	24.56	1.96
Wheat straw-activated carbon	82.87	5.89	3.21	6.82	1.21
Corn cob	58.76	8.90	10.83	20.54	.97
Corn cob-activated carbon	88.54	2.56	1.89	6.45	.56

samples. Activated carbon's surface area is essential in practical application as an adsorbent. The investigations are performed at a temperature of about 77 K, and a relative pressure varies from 0 to 1 bar pressure. Before the experimentation, all activated carbon samples are placed in a sample-holding container. The degassed is achieved by maintaining at a temperature of about 120 °C for 45 min. After that, samples are further degassed to retain at 250 °C for nearly 12 h to remove moisture content. Figure 1 depicts the N_2 adsorption/desorption curves of activated carbon samples.

It can be apparent from the figure that all activated carbon samples exhibit a similar pattern of adsorption and desorption curves. It shows the path of the reversible process. Based on International Union Pure and Applied Chemistry (IUPAC) classification for adsorption isotherms, all samples exhibit the same Type IV adsorption isotherm. The curves resemble a hysteresis loop, which suggests the monolayer followed by multilayer formation (Ref 11). In addition, all adsorbent samples exhibit an increasing trend by $P/P_0 = 0.1$, which corresponds to the higher active pores and excellent surface area. The adsorbent samples' average pore diameter (D_p) is determined using the surface area (S) and pore volume (V_T).

$$D_P = 4V_T/S \quad \text{(Eq 2)}$$

It is understood from the literature that the adsorbent possesses excellent surface area, and pore volume is more significant for gas adsorption and surface diffusion rate. Similarly, activated carbon samples have more active adsorptive pore sites on their surface, thus enable for better adsorption performance (Ref 20, 21). The average pore width of the adsorbent sample range between 1 and 2.5 nm, which is more suitable for gas-phase applications (Ref 12). As a result of activation, adsorbent samples would enhance the number of

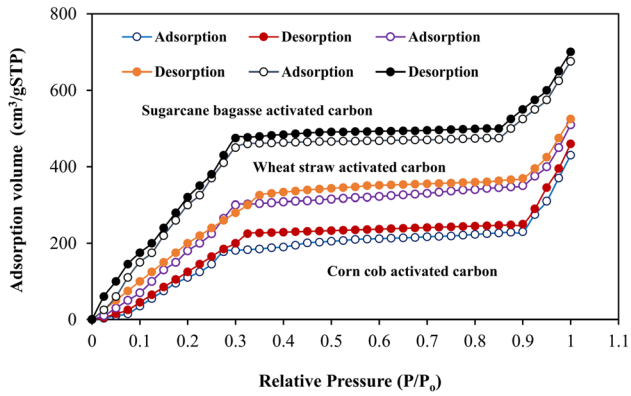

Fig. 1 N_2 adsorption–desorption isotherms of activated carbon samples

active adsorptive pores sites for physical adsorption. The porosity is another essential factor for activated carbon, which enhances its adsorption in real-time applications (Ref 22). Pore size distribution of adsorbent samples is studied using Non-local Density Functional Theory (NLDFT) through the slit pores, and the findings are shown in Fig. 2.

It is noticed that all adsorbent samples possess a well-defined carbon structure with numerous pores. Thus, CO_2 molecules can occupy available spaces on adsorbents, which facilitates physical gas adsorption (Ref 6). The formation of different pore sizes is mainly attributed to the single-stage activation process. The curves are well-suited for non-homogeneous adsorbents like activated carbon, which account for effective surface curvature and more energetic adsorption pore sites. Due to the hierarchical nature of adsorbent samples with

micropores-mesopores, samples are more significant for effective CO_2 physical adsorption. The presence of micropores confirms a greater potential for CO_2 adsorption.

It can be inferred from experimentation that the availability of narrow micropores on adsorbent samples is mainly responsible for good CO_2 adsorption at atmospheric pressure conditions. Meanwhile, efficient surface area and wide pores are vital for excellent CO_2 adsorption under high-pressure conditions (Ref 19, 23). Hence, biomass-based adsorbent samples are crucial for CO_2 capture applications in ambient and temperature conditions and maximal pressure conditions (post-combustion adsorption-based carbon capture system).

3.3 SEM Analysis

Biomass-based adsorbent samples are characterized and analyzed to investigate surface morphology, microscopy structure, and surface topology (Ref 24). It provides detailed high-resolution micrographic images of the sample. SEM analysis is performed at an accelerating voltage of 15 kV under various magnification factors. Before the analysis, all adsorbent samples are placed in a muffle furnace at a temperature of 100 °C for 2 h. Further, they are kept in a vacuum desiccator to remove moisture content from adsorbent samples' surface. Figure 3(a)-(c) shows SEM micrographic images of activated carbon samples.

It can be observed from figures that all adsorbent samples exhibit a broad and accessible porous structure on their surface. This is mainly achieved due to the single-stage activation process. The porous structures of biomass-based adsorbents on their surface show distinctive shapes and sizes. Thus, the various form of porous networks can be termed heterogeneous. The porous structure of samples more significantly facilitates the surface diffusion of CO_2 to active adsorptive pores, which confirms the physical adsorption (Ref 25). The distinct pore sizes with irregular surface area, as seen in sugarcane bagasse-, wheat straw-, and corn cob-activated carbon samples, respectively. Apart from these, activated carbon samples should possess heterogeneous pores with multiple cracks, cavities, voids, and gaps on their surface. This may be achieved due to a suitable chemical activating agent used for chemical activation. As result of the activation process, which ensures the development of effective pores on the surface of activated carbon samples. The greater surface area with higher active adsorptive pore sites of adsorbents corresponds to superior CO_2 adsorption (Ref 26, 27).

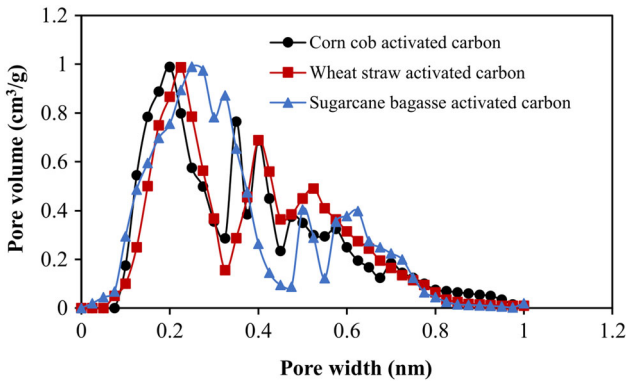

Fig. 2 Pore size distribution of activated carbon samples

3.4 FTIR Analysis

Activated carbon samples' surface chemical functional groups are analyzed using FTIR at a wavelength of 400-4000 cm^{-1}. The carbon matrix comprises heteroatoms other than carbon atoms, including nitrogen, oxygen, hydrogen, halogen, sulfur, phosphorus, and others (Ref 28) (Ref 29). Activated carbons' surface chemistry is controlled by these heteroatoms, which are bound to the margins of the carbon layers. FTIR spectra give detailed information about the chemical structure on the surface of activated carbon. The FTIR spectra of activated carbon obtained from three different biomass are shown in Fig. 4(a)-(c).

It can be observed from the figure that the spectra of activated carbon samples with their peaks show the existing functional groups on their surface. In the sugarcane bagasse-activated carbon sample, the peak at 2785-3992 cm^{-1} is assigned to O-H groups. Similarly, the peaks at 1256-1835 and 2175-2740 cm^{-1} correspond to C-O and C=O groups, respectively. A broad stretching of the band at 3022-3919 cm^{-1} belongs to O-H groups. The sharp bands observed at 1708-2303, and 930-1324 cm^{-1} are assigned to C-O and COOH groups for wheat straw-activated carbon. A wide transmittance band, at 3120-3890 cm^{-1}, can be allocated to the O-H stretching mode of hydroxyl groups. Sharp spectra bands at 1820-2252 and 1094-1243 cm^{-1} correspond to the vibrations of carbonated and carboxyl groups, respectively, for the corn cob-based activated carbon sample. All activated carbon samples' spectrum and their specific chemical surface groups present on their surface may contribute to the adsorption performance (Ref 30, 31).

Mass fractions of C, O, and N and other heteroatoms are quantified using CHNS/O analysis to examine the elemental composition of adsorbent samples. The ultimate analysis is carried out using a CHNS/O analyzer. The study confirms the highest carbon percentage, which ensures CO_2 adsorption suitability. The chemical impregnation on the surface of raw materials may trigger surface chemistry and develop pore and pore structures on derived samples. The biomass-based adsorbent samples have the maximum percentage of carbon as compared to other elemental compositions. This may be attributed to CO_2 physical adsorption of adsorbent samples.

3.5 TGA Analysis

Thermogravimetric analysis (TGA) is mainly used to examine the sample's thermal decomposition, kinetic reaction, and chemical composition (Ref 32, 33). The TGA profile of activated carbon samples is shown in Fig. 5.

It can be apparent from the figure that samples' thermal degradation occurs over the increment of temperature. Three stages of thermal degradation occur for all activated carbon samples. In the 1st stage of thermal degradation, moisture content completely evaporated at a temperature range between 50 and 150 °C for all activated carbon samples. During 2nd stage of thermal degradation, at a temperature of 175-500 °C, samples tend to lose their mass. This thermal event occurs in moderate degradation with a mass loss of 25-40%. At the 3rd stage of thermal degradation, at a temperature of 550-700 °C, samples' attain 85-90% of mass loss. Therefore, it can be affirmed that all activated carbon samples can be used for adsorption. It is noticed from the TGA results and proximate analysis that a minimum ash content is observed for all

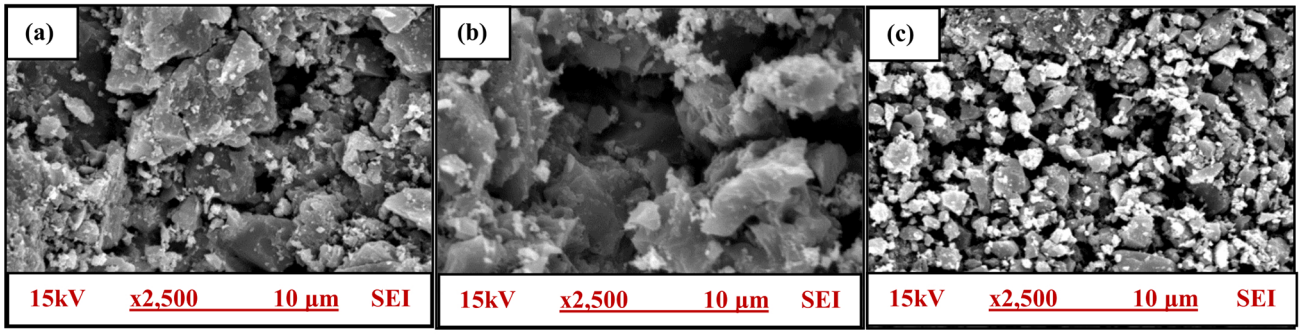

Fig. 3 SEM micrographic images of (a) sugarcane bagasse-activated carbon; (b) wheat straw-activated carbon; and (c) corn cob-activated carbon

activated carbon samples. It is one of the essential characteristics for selecting suitable candidates for activated carbon preparation.

All adsorbent samples confirm excellent surface characteristics and physicochemical properties from characterization results. Thus, these potential adsorbents play a significant role in CO_2 adsorption.

4. CO_2 Capture Assays

4.1 CO_2 Uptake of Activated Carbon Samples

In post-combustion CO_2 capture, the flue gas consists of CO_2 and N_2 in ambient conditions. CO_2 partial pressure is in the 0.01-0.1 bar range. Furthermore, the flue gas temperature is relatively maximum, about 75-175 °C. The adsorption process is not well-suited to such maximum temperature conditions. Thus, the adsorbent will capture minimum CO_2 molecules capture/uptake (Ref 34). It is understood from the existing literature that in the post-combustion adsorption-based CO_2 capture system, the flue gas is initially cooled down to a minimum temperature and then passed to the capture unit for the adsorption process. Hence, the present investigation is performed at a temperature of about 0-90 °C and a pressure of about 0.1-1 bar. The experimental findings of the adsorption–desorption isotherms of adsorbent samples under different operating conditions are given in Fig. 6(a)-(c).

It can be apparent from figures that all activated carbon samples exhibit maximum CO_2 adsorption with an increase in pressure under all temperature conditions. On the other hand, a drop in CO_2 adsorption is observed for all activated carbon samples with a raising temperature. This may be due to the reduction in binding strength and Van der Waal forces of attraction between the solid adsorbent and the adsorbate CO_2 molecules (Ref 35, 36). At maximum temperature, more adsorption energy is required for molecular diffusion on the adsorbent sample surface. Thus, adsorbate CO_2 molecules completely detaches from the surface of the adsorbent sample. The process is known as desorption. The significant reduction in the CO_2 adsorption potential of adsorbent samples at maximum temperature is mainly associated with their internal energy (Ref 37). Therefore, adsorbed CO_2 molecules are liberated from the active adsorptive pore sites on the surface of adsorbent samples. Thus, results of the surface phenomena of adsorbents show a spontaneous exothermic reaction, which indicates the physical adsorption mechanism.

It is noticed that there is good interaction between adsorbent samples and the adsorbate CO_2 molecules. This is mainly due to the minimum temperature and optimum pressure conditions. As a result, adsorbent samples exhibit multilayer formation. Thus, obtaining maximum CO_2 uptake on the surface of adsorbent samples at a minimum temperature and maximum pressure is essential, as gas streams from different sources are cooled down under ambient conditions. All adsorbent samples' adsorption isotherms resemble Type IV curves. It corresponds to the hysteresis curve, which follows monolayer with multilayer formation (Ref 38). It is observed that the sugarcane bagasse-activated carbon sample exhibits maximum CO_2 uptake of 6.25, 5.3, 4.2, and 2.15 mmol g^{-1} at 0, 30, 60, and 90 °C, respectively. Similarly, wheat straw- and corn cob-activated carbons show maximum CO_2 uptake of 5.85, 4.4, 3.3, and 1.45 mmol g^{-1}, and 5.25, 4.0, 3.2, and 1.2 mmol g^{-1} at 0, 30, 60, and 90 °C, respectively. This is mainly due to the active pore sites, good CO_2 selectivity, excellent surface morphology, and surface chemistry (Ref 23, 39, 40).

It is noted that sugarcane bagasse- and wheat straw-activated carbon samples exhibit maximum CO_2 uptake at operating conditions, whereas corn cob-activated carbon sample shows moderate CO_2 uptake. This is primarily due to adsorbent samples' porosity, surface area, and suitable working conditions (Ref 41). The highest CO_2 uptake at 0 °C is noticed for sugarcane bagasse and wheat straw adsorbents because of the reasonable BET surface area and micropore volume. Corn cob adsorbent exhibits moderate adsorption capacity. This can be attributed to the effective pores and surface affinity. In the investigation, it can be mentioned that pore sizes are essential as the CO_2 adsorption process that occurs is physical adsorption due to Van der Waal's forces of attraction (Ref 40, 42). During physical adsorption, the interaction energy between adsorbent surface functionalities and adsorbate molecules. Hence, it can be noticed that the performance of these adsorbent samples can be used for post-combustion CO_2 capture applications.

4.2 CO_2 and N_2 Adsorption Isotherms of Activated Carbon Samples

This investigation evaluates adsorbent samples to determine CO_2 and N_2 adsorption isotherms at a suitable operating condition of about 0 °C and 1 bar. Figure 7(a)-(c) shows activated carbon samples' CO_2 and N_2 adsorption isotherms.

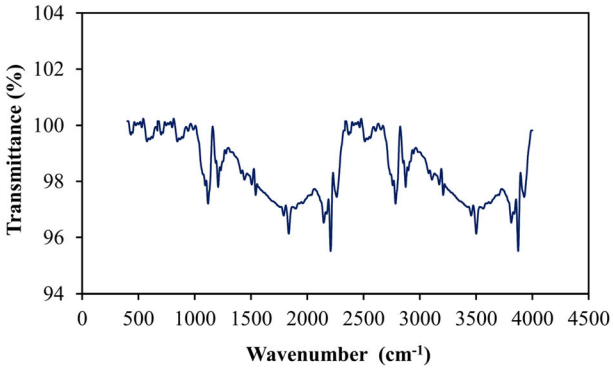

(a)

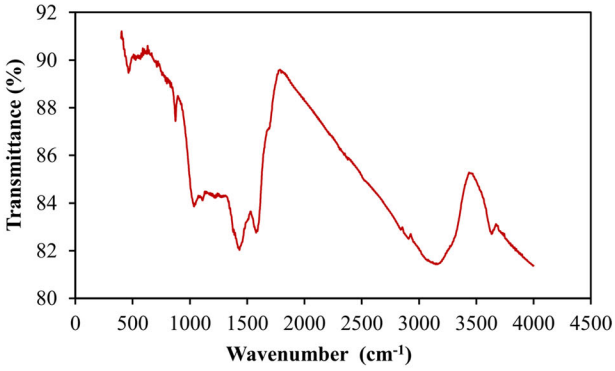

(b)

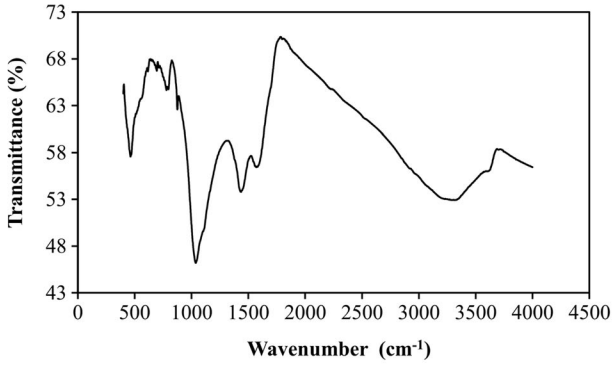

(c)

Fig. 4 FTIR spectra of activated carbon samples. (a) Sugarcane bagasse-activated carbon. (b) Wheat straw-activated carbon. (c) Corn cob-activated carbon

It is observed from figures that the adsorption isotherms of both gas molecules increase with an increase in pressure. The adsorption isotherm of N_2 uptake is lower than CO_2 uptake for all activated carbon samples. This is mainly due to the selective nature (i.e., CO_2/N_2 selectivity), porosity properties, and surface functional groups of activated carbon samples (Ref 14). The plot of all activated carbon samples reveals that the availability of adsorption sites on their surface enhances faster adsorption kinetics rate. Thus, activated carbon samples can be used for industrial applications.

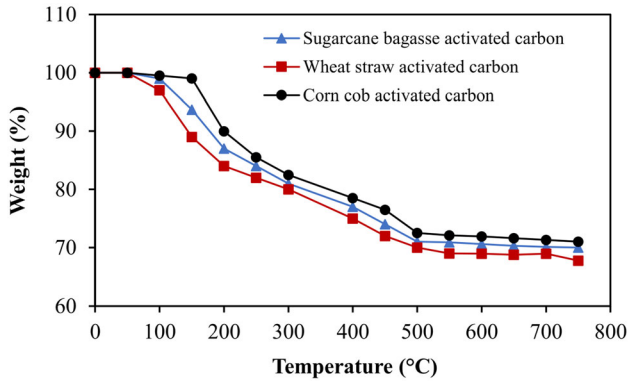

Fig. 5 TGA analysis of activated carbon samples

4.3 Cyclic Study of CO_2 Adsorption for Activated Carbon Samples

In the analysis, the reusability and recyclability of CO_2 adsorption isotherm is the most crucial parameter for real-time practical application. About four adsorption/desorption test cycles of activated carbon samples are investigated using the same samples for continuous test cycles. The original activated carbon samples are regenerated using a temperature swing adsorption (TSA) approach (Ref 7). The adsorption capacity of activated carbon samples is examined at suitable operating conditions of about 0 °C and 1 bar. Figure 8(a)-(c) displays the cyclic adsorption performance of all activated carbon samples. It is observed from figures that the adsorption capacity of activated carbon samples reduces slightly over continuous test cycles. This may be due to the accumulation of adsorbate molecules on the surface of activated carbon that has not been released completely. It is noticed that a slight drop of about 4% loss of CO_2 uptake takes place for activated carbon samples by continuous cyclic tests. This may be the closure of active pore sites on activated carbon samples (Ref 13, 15). The test cycle indicates that all activated carbon samples exhibit superior adsorption performance on multiple adsorption–desorption test cycles. Thus, activated carbon can be used for actual practical applications.

4.4 Breakthrough Curve

Acivated carbon's dynamic CO_2 uptake can easily be obtained from the breakthrough curve. It is an essential parameter for adsorption (Ref 43). Figure 9 depicts the breakthrough curves of activated carbon samples.

C/C_0 refers to the ratio of outlet CO_2 concentration to inlet CO_2 concentration as an adsorption time duration. It is observed from the figure that the adsorption of CO_2 loading on activated carbon samples. After that, activated carbon reaches saturation point (Ref 11). By interpreting the breakthrough plots, a dynamic CO_2 capture capacity of 0.65, 0.76, and 0.89 mmol/g is achieved for corn cob-, wheat straw-, and sugarcane bagasse-activated carbon samples, respectively.

4.5 Isosteric Heat of Adsorption

The isosteric heat of adsorption ($\triangle H_{ads}$) is an essential parameter for CO_2 adsorption. It is mainly used to investigate the adsorbent-adsorbate interaction (Ref 44). The calculations of $\triangle H_{ads}$ values are done by using the Clausius–Clapeyron equation. Figure 10 illustrates the isosteric heat of adsorption of

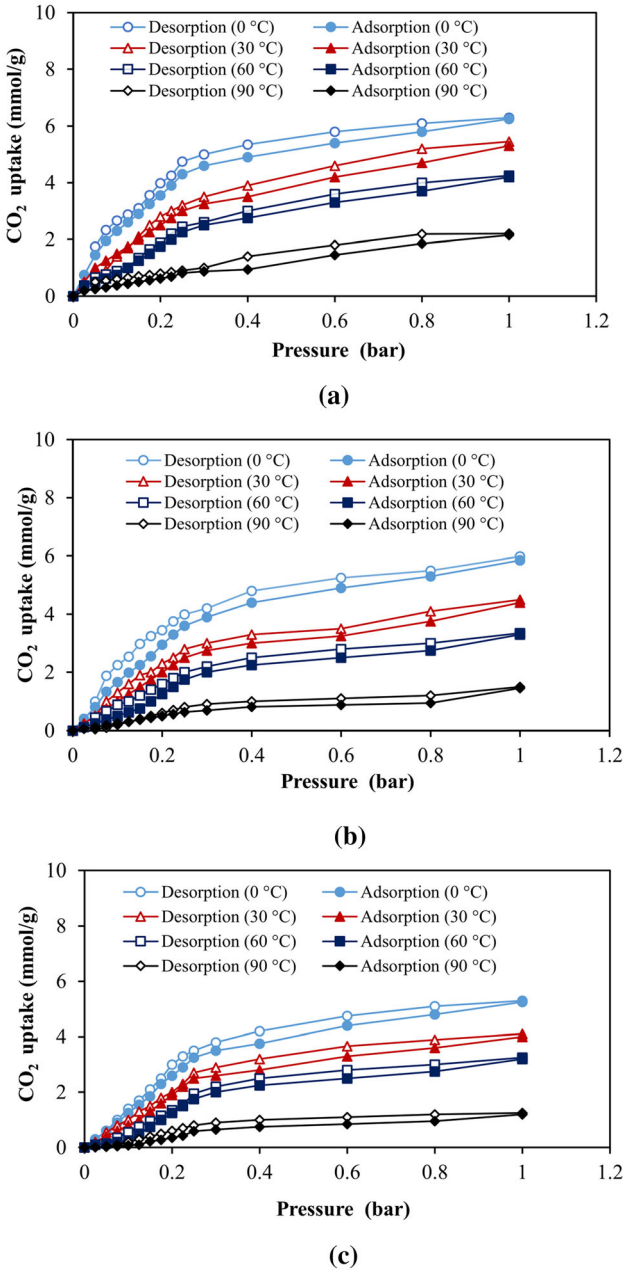

Fig. 6 CO_2 adsorption–desorption isotherms of activated carbon samples. (a) Sugarcane bagasse-activated carbon. (b) Wheat straw-activated carbon. (c) Corn cob-activated carbon

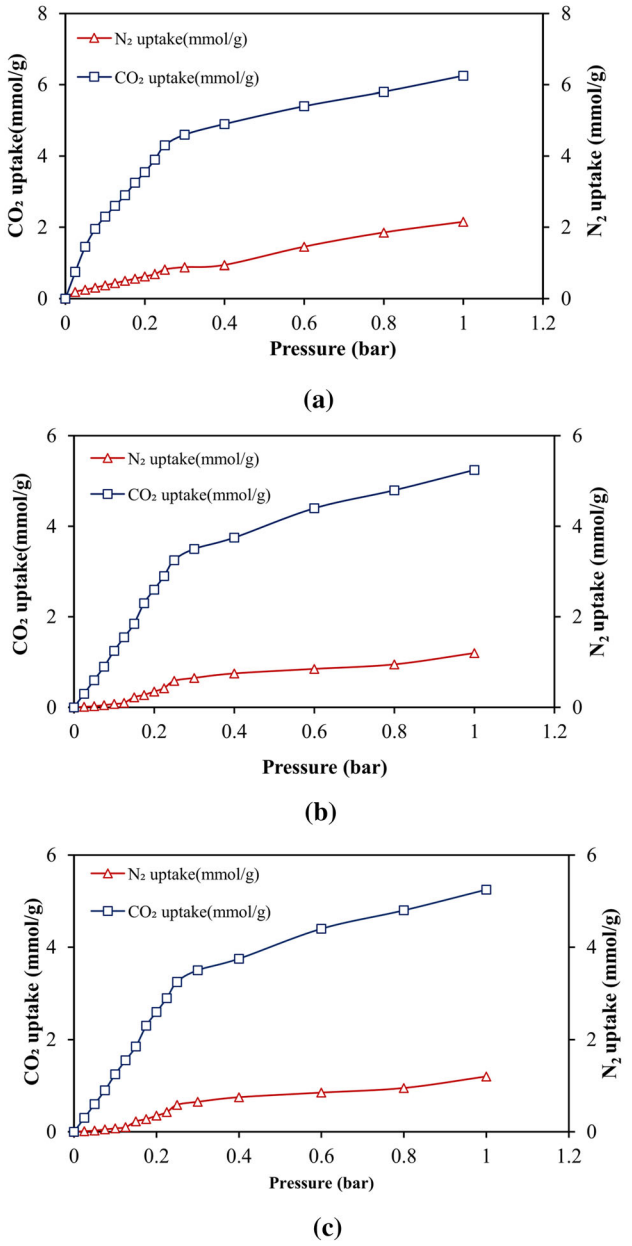

Fig. 7 CO_2 and N_2 adsorption isotherms of activated carbon samples. (a) Sugarcane bagasse-activated carbon. (b) Wheat straw-activated carbon. (c) Corn cob-activated carbon

activated carbon samples concerning the amount of CO_2 adsorbed.

It can be apparent from the figure that isosteric heat is achieved at the highest of about 35.5 kJ mol^{-1} for the sugarcane bagasse-activated carbon sample. This ensures the strong interaction between CO_2 accumulated on the surface of activated carbon sample. The highest values of $\triangle H_{ads}$ are 30, and 24 kJ mol^{-1} for wheat straw- and corn cob-activated samples, respectively. This can be affirmed that there is a slightly weak interaction between adsorbents and adsorbate molecules (Ref 45).

For the sugarcane bagasse-activated carbon sample, $\triangle H_{ads}$ occur in the range of 35.5-21.5 kJ mol^{-1}, whereas $\triangle H_{ads}$ occur in the range of 30-17 kJ mol^{-1} for the wheat straw-activated sample and $\triangle H_{ads}$ occur in the range of 27-14 kJ mol^{-1} for the corn cob-activated sample. It is noted that with an increase in CO_2 uptake, $\triangle H_{ads}$ decrease gradually. This is because of the drastic occupation of adsorptive pores on the surface of samples (Ref 38). All activated carbon samples exhibit superior adsorption performance, which indicates exothermic reaction and spontaneity of nature. The values of $\triangle H_{ads}$ for all activated carbon samples are within the range of ordinary physisorption (< 40 kJ mol^{-1}), which indicates samples take place physical adsorption process (Ref 46, 47).

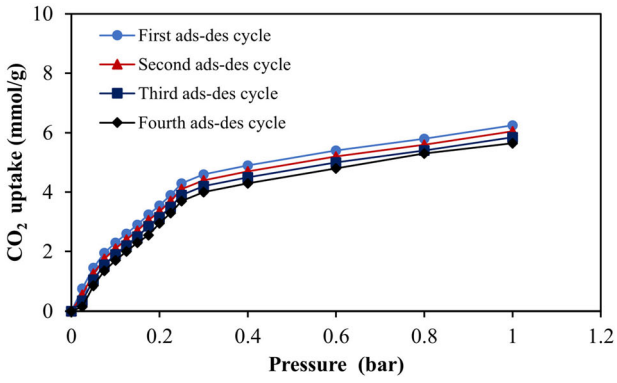

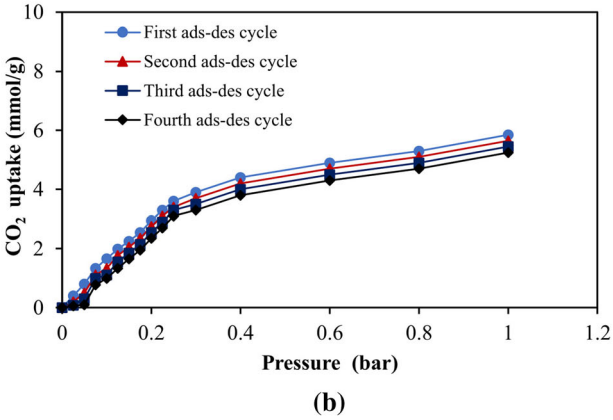

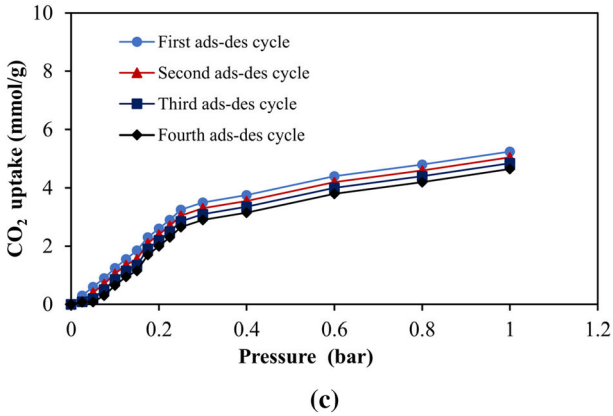

Fig. 8 Cyclic study of CO_2 adsorption for activated carbon samples. (a) Sugarcane bagasse-activated carbon. (b) Wheat straw-activated carbon. (c) Corn cob-activated carbon

4.6 Surface Textural Properties and Porous Structure Characteristics on CO_2 Uptake

The present study context primarily emphasizes textural characteristics and surface properties that are significant for CO_2 adsorption performance or gas storage (Ref 48). Thus, it is essential to characterize surface porous, morphology, and texture of the adsorbent sample. The surface textural characteristics and physical and chemical properties of adsorbents play a crucial role in effective CO_2 physical adsorption under ambient conditions (Ref 38, 49). CO_2 adsorption mainly depends on textural features, such as the surface area and total pore volume of the adsorbent. The surface textural properties

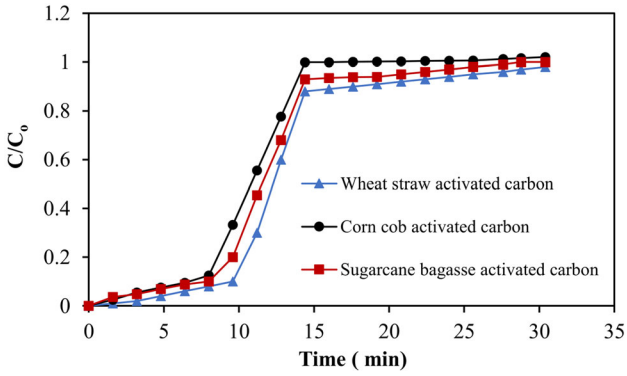

Fig. 9 Breakthrough curve

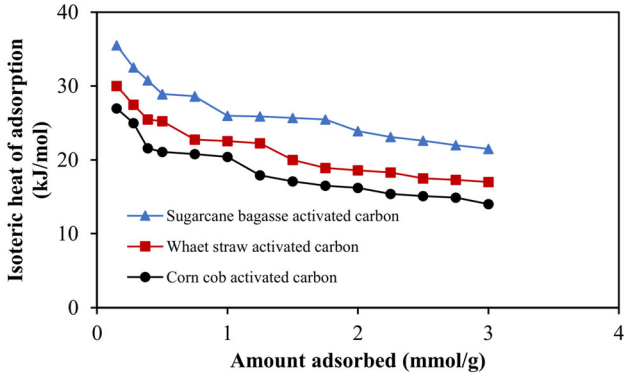

Fig. 10 Isosteric heat of adsorption of activated carbon samples

and physicochemical characteristics of adsorbent samples are tabulated in Table 4.

4.7 Significance of Present Study and Scope for Future Work

The current investigation highlights the different analytical characterizations and the maximum CO_2 adsorption isotherm of biomass-based adsorbents. The prominence of the research work is not only the preparation of activated carbons from abundantly available and inexpensive biomass sources. It is also the exploration of physicochemical characteristics and surface textural properties of the developed adsorbent. Moreover, an extensive investigation is done on producing adsorbents from different biomass residues with maximum CO_2 uptake. Hence, the present research is crucial to using adsorbents for post-combustion adsorption-based carbon capture applications. Physical adsorption is a surface phenomenon, a spontaneous exothermic reaction, and efficient removal of heat released on adsorbent during adsorption-based CO_2 capture (Ref 12). Based on the adsorbents' adsorption performance, the adsorbent capture unit is designed and developed for practical applications. The analytical and characterization data of the adsorbent would provide a precise scenario of real-time practicality of carbon capture.

4.8 A Short Note on Potential Adsorbents for Carbon Capture

Besides these biomass-based adsorbents, numerous biomass sources can be used as feedstock for CO_2 physical adsorption to

Table 4 Surface textural properties and physicochemical characteristics of adsorbent samples

Activated carbon sample	Surface textural characteristics		CO_2 adsorption capacity, mmol g^{-1}			
	S_{BET}, m^2/g	V_T, cm^3/g	0 °C	30 °C	60 °C	90 °C
Sugarcane bagasse-activated carbon	2348	1.69	6.35	5.3	4.2	2.15
Wheat straw-activated carbon	1945	0.89	5.85	4.4	3.3	1.45
Corn cob-activated carbon	1654	0.75	5.25	4.0	3.2	1.2

meet net-zero emissions. Many studies documented in the literature on doped adsorbents and composite adsorbents confirm their superior adsorption performance. Few recent investigations have been reported on the activation temperature and impregnation ratio. This would enhance the surface texture properties and physicochemical properties of derived adsorbents. Thus, adsorbents exhibit excellent CO_2 uptake in adsorption-based applications under suitable operating conditions. Therefore, biomass-based adsorbent is an effective way of waste minimization and sequestration of hazardous pollutants in post-combustion CO_2-based adsorption systems (Ref 6, 7, 11).

5. Conclusions

In the present study, the preparation and characterization of three biomass-activated carbons, namely (i) corn cob-activated carbon, (ii) sugarcane bagasse-activated carbon, and (iii) wheat straw-activated carbon, are performed to examine CO_2 capture at operating conditions. Physicochemical characteristics and surface textural properties of the developed activated carbon samples are evaluated. Active pore sites, surface functional groups, and thermal stability of activated carbon samples are also determined and discussed. The findings are given as follows:

- Inexpensive and abundantly available feedstocks are used to prepare activated carbons using single-stage activation.
- The developed activated carbon samples are subjected to different characterizations to examine their feasibility of CO_2 adsorption.
- At 1 bar and 0 °C, activated carbon exhibits maximum CO_2 uptake of 5.85, 5.25, and 6.25 mmol g^{-1} for wheat straw, corn cob, and sugarcane bagasse adsorbents, respectively.
- All activated carbon samples exhibit superior adsorption performance on multiple adsorption–desorption test cycles.
- A dynamic CO_2 capture capacity of 0.65, 0.76, and 0.89 mmol/g is achieved for corn cob-, wheat straw-, and sugarcane bagasse-activated carbon samples, respectively.
- All activated carbon samples show excellent CO_2 uptake and moderate N_2 uptake with CO_2/N_2 selectivity.
- $\triangle H_{ads}$ values of the adsorbents are 30-17, 27-14, and 35.5-21.5 kJ mol^{-1} for wheat straw, corn cob, and sugarcane bagasse adsorbents, respectively. It ensures that the adsorption process is physical adsorption, exothermic, and spontaneous.
- All adsorbent samples exhibit superior adsorption capability and excellent adsorption performance.
- The developed adsorbents are appropriate for gas sorption applications and can be used in carbon capture, gas separation, and energy storage systems.
- The current study affirms that CO_2 physical adsorption is of prime importance at minimum temperature and maximum pressure, apart from surface textural properties and physicochemical characteristics.

References

1. M. Songolzadeh, M. Soleimani, M.T. Ravanchi, and R. Songolzadeh, Carbon Dioxide Separation from Flue Gases: A Technological Review Emphasizing Reduction in Greenhouse Gas Emissions, *Sci. World J.*, 2014, **2014**, p 1–34. https://doi.org/10.1155/2014/828131
2. B.P. Spigarelli and S.K. Kawatra, Opportunities and Challenges in Carbon Dioxide Capture, *J. CO2 Util.*, 2013, **1**, p 69–87. https://doi.org/10.1016/j.jcou.2013.03.002
3. A. Al-Mamoori, A. Krishnamurthy, A.A. Rownaghi, and F. Rezaei, Carbon Capture and Utilization Update, *Energy Technol.*, 2017, **5**(6), p 834–849
4. S.-i Nakao, K. Yogo, K. Goto, T. Kai, and H. Yamada, *Advanced CO2 Capture Technologies: Absorption, Adsorption, and Membrane Separation Methods*, Springer International Publishing, Cham, 2019
5. M.K. Al Mesfer, Synthesis and Characterization of High-Performance Activated Carbon from Walnut Shell Biomass for CO_2 Capture, *Environ. Sci. Pollut. Res.*, 2020, **27**(13), p 15020–15028
6. R. Maniarasu, S.K. Rathore, and S. Murugan, Biomass-Based Activated Carbon for CO_2 Adsorption–A Review, *Energy Environ.*, 2022 https://doi.org/10.1177/0958305X221093465
7. M. Ravi, S.K. Rathore, and M. Sivalignam, Experimental Investigation on Using Adsorbent for Post-Combustion Carbon Dioxide Capture from CI Engine Exhaust, *Environ. Prog. Sustain. Energy*, 2022 https://doi.org/10.1002/ep.13987
8. S. Ding and Y. Liu, Adsorption of CO_2 from Fl Ue Gas by Novel Seaweed-Based KOH-Activated Porous Biochars, *Fuel, Elsevier*, 2020, **260**, p 116382. https://doi.org/10.1016/j.fuel.2019.116382
9. I.S. Ismail, N.A. Rashidi, and S. Yusup, Production and Characterization of Bamboo-Based Activated Carbon through Single-Step H_3PO_4 Activation for CO_2 Capture, *Environ. Sci. Pollut. Res.*, 2022, **29**(9), p 12434–12440
10. X.X. Wu, C.Y. Zhang, Z.W. Tian, and J.J. Cai, Large-Surface-Area Carbons Derived from Lotus Stem Waste for Efficient CO_2 Capture, *Xinxing Tan Cailiao/New Carbon Mater.*, 2018, **33**(3), p 252–261. https://doi.org/10.1016/S1872-5805(18)60338-5
11. R. Maniarasu, S.K. Rathore, and S. Murugan, Preparation, Characterization, and Performance of Activated Carbon for CO_2 Adsorption from CI Engine Exhaust, *Greenh. Gases Sci. Technol.*, 2022, **12**(2), p 284–304
12. S.S. Gautam, Experimental Investigation on Different Activated Carbons as Adsorbents for CO_2 Capture, *Therm. Sci. Eng. Progr.*, 2022, **33**, p 101339. https://doi.org/10.1016/j.tsep.2022.101339
13. J. Huang, J. Bai, M. Demir, X. Hu, Z. Jiang, and L. Wang, Efficient N-Doped Porous Carbonaceous CO_2 Adsorbents Derived from Commer-

cial Urea-Formaldehyde Resin, *Energy Fuels*, 2022, **36**(11), p 5825–5832
14. C. Ma, J. Bai, M. Demir, H. Xin, S. Liu, and Linlin Wang, Water Chestnut Shell-Derived N/S-Doped Porous Carbons and Their Applications in CO_2 Adsorption and Supercapacitor, *Fuel*, 2022, **326**, p 125119. https://doi.org/10.1016/j.fuel.2022.125119
15. L. Tingyan, J. Bai, M. Demir, H. Xin, J. Huang, and L. Wang, Synthesis of Potassium Bitartrate-Derived Porous Carbon via a Facile and Self-Activating Strategy for CO_2 Adsorption Application, *Sep. Purif. Technol.*, 2022, **296**, p 121368. https://doi.org/10.1016/j.seppur.2022.121368
16. V.E. Efeovbokhan, E.E. Alagbe, B. Odika, R. Babalola, T.E. Oladimeji, O.G. Abatan, and E.O. Yusuf, Preparation and Characterization of Activated Carbon from Plantain Peel and Coconut Shell Using Biological Activators, *J. Phys. Conf. Ser.*, 2019, **1378**(3), p 032035. https://doi.org/10.1088/1742-6596/1378/3/032035
17. O.A. Babatunde, S. Garba, and Z.N. Ali, Surface Modification of Activated Carbon for Improved Iodine and Carbon Tetrachloride Adsorption, *Am. J. Chem.*, 2016, **6**(3), p 74–79. https://doi.org/10.5923/j.chemistry.20160603.02
18. S. Maulina and M. Iriansyah, Characteristics of Activated Carbon Resulted from Pyrolysis of the Oil Palm Fronds Powder, *IOP Conf. Ser. Mater. Sci. Eng.*, 2018, **309**, p 012072. https://doi.org/10.1088/1757-899X/309/1/012072
19. Y.X. Gan, Activated Carbon from Biomass Sustainable Sources, *C (Basel)*, 2021, **7**(2), p 39
20. M. Song, B. Jin, R. Xiao, L. Yang, Y. Wu, Z. Zhong, and Y. Huang, The Comparison of Two Activation Techniques to Prepare Activated Carbon from Corn Cob, *Biomass Bioenergy*, 2013, **48**, p 250–256
21. J. Guo and A.C. Lua, Textural and Chemical Properties of Adsorbent Prepared from Palm Shell by Phosphoric Acid Activation, *Mater. Chem. Phys.*, 2003, **80**(1), p 114–119
22. E. Misran, O. Bani, E.M. Situmeang, and A.S. Purba, Banana Stem Based Activated Carbon as a Low-Cost Adsorbent for Methylene Blue Removal: Isotherm, *Kinet. Reusab. Alexandria Eng. J.*, 2022, **61**(3), p 1946–1955
23. A. Toprak and T. Kopac, Carbon Dioxide Adsorption Using High Surface Area Activated Carbons from Local Coals Modified by KOH, NaOH and $ZnCl_2$ Agents, *Int. J. Chem. React. Eng.*, 2017 https://doi.org/10.1515/ijcre-2016-0042
24. M. Ilomuanya, B. Nashiru, N. Ifudu, and C. Igwilo, Effect of Pore Size and Morphology of Activated Charcoal Prepared from Midribs of Elaeis Guineensis on Adsorption of Poisons Using Metronidazole and Escherichia Coli O157:H7 as a Case Study, *J. Microsc. Ultrastruct.*, 2017, **5**(1), p 32. https://doi.org/10.1016/j.jmau.2016.05.001
25. I. Demiral and C. Aydin Şamdan, Preparation and Characterisation of Activated Carbon From Pumpkin Seed Shell Using H_3PO_4, *Anadolu Univ. J. Sci. Technol. A Appl. Sci. Eng.*, 2016, **17**(1), p 125–138
26. F. Hussin, M.K. Aroua, and R. Yusoff, Adsorption of CO_2 on Palm Shell Based Activated Carbon Modified by Deep Eutectic Solvent: Breakthrough Adsorption Study, *J. Environ. Chem. Eng.*, 2021, **9**(4), p 105333. https://doi.org/10.1016/j.jece.2021.105333
27. N.K.E.M. Khori, T. Hadibarata, M.S. Elshikh, A.A. Al-Ghamdi, and Z.Y. Salmiati, Triclosan Removal by Adsorption Using Activated Carbon Derived from Waste Biomass: Isotherms and Kinetic Studies, *J. Chin. Chem. Soc.*, 2018, **65**(8), p 951–959. https://doi.org/10.1002/jccs.201700427
28. J. Bedia, M. Peñas-Garzón, A. Gómez-Avilés, J. Rodriguez, and C. Belver, A Review on the Synthesis and Characterization of Biomass-Derived Carbons for Adsorption of Emerging Contaminants from Water, *C*, 2018, **4**(4), p 63. https://doi.org/10.3390/c4040063
29. G.K. Latinwo and S.E. Agarry, Removal of Phenol from Paint Wastewater by Adsorption Onto Phosphoric Acid Activated Carbon Produced from Coconut Shell: Isothermal and Kinetic Modelling Studies, *Chem. Mater. Res.*, 2015, **7**(5), p 123–138
30. D. Prahas, Y. Kartika, N. Indraswati, and S. Ismadji, Activated Carbon from Jackfruit Peel Waste by H_3PO_4 Chemical Activation: Pore Structure and Surface Chemistry Characterization, *Chem. Eng. J.*, 2008, **140**(1–3), p 32–42
31. K.S. Ukanwa, K. Patchigolla, R. Sakrabani, E. Anthony, and S. Mandavgane, A Review of Chemicals to Produce Activated Carbon from Agricultural Waste Biomass, *Sustainability (Switzerland)*, 2019, **11**(22), p 1–35
32. L. Giraldo, P. Rodriguez-Estupiñán, and J.C. Moreno-Piraján, Isosteric Heat: Comparative Study between Clausius–Clapeyron, CSK and Adsorption Calorimetry Methods, *Processes*, 2019, **7**(4), p 203. https://doi.org/10.3390/pr7040203
33. D.P. Bezerra, R.S. Oliveira, R.S. Vieira, C.L. Cavalcante, and D.C.S. Azevedo, Adsorption of CO_2 on Nitrogen-Enriched Activated Carbon and Zeolite 13X, *Adsorption*, 2011, **17**(1), p 235–246
34. M. Musah, Y. Azeh, J. Mathew, M. Umar, Z. Abdulhamid, and A. Muhammad, Adsorption Kinetics and Isotherm Models: A Review, *Caliphate J. Sci. Technol.*, 2022, **4**(1), p 20–26
35. P. Murge, S. Dinda, and S. Roy, Adsorbent from Rice Husk for CO_2 Capture: Synthesis, Characterization, and Optimization of Parameters, *Energy Fuels*, 2018, **32**(10), p 10786–10795
36. J. Wang and X. Guo, Adsorption Isotherm Models: Classification, Physical Meaning, Application and Solving Method, *Chemosphere*, 2020, **258**, p 127279
37. C. Dinca, N. Slavu, A. Badea, N. Slavu, and A. Badea, CO_2 Adsorption Process Simulation in ASPEN Hysys, in *Proceedings of 8th International Conference on Energy and Environment: Energy Saved Today is Asset for Future, CIEM 2017*, 2017, p 505–509
38. X. Liu, C. Sun, H. Liu, W.H. Tan, W. Wang, and C. Snape, Developing Hierarchically Ultra-Micro/Mesoporous Biocarbons for Highly Selective Carbon Dioxide Adsorption, *Chem. Eng. J.*, 2018, **2019**(361), p 199–208
39. E.M. Calvo-muñoz, F.J. García-mateos, and J.M. Rosas, Biomass Waste Carbon Materials as Adsorbents for CO_2 Capture under Post-Combustion Conditions, *Front. Mater.*, 2016, **3**, p 1–14
40. S. Chowdhury and S. Pan, *Biomass-Derived Microporous Adsorbents for Selective CO2 Capture*, Elsevier Inc., Microbial and Natural Macromolecules, 2021
41. S.M. Hong, E. Jang, A.D. Dysart, V.G. Pol, and K.B. Lee, CO_2 Capture in the Sustainable Wheat-Derived Activated Microporous Carbon Compartments, *Sci Rep.*, 2016, **6**(September), p 1–10
42. M. Bernardo, N. Lapa, I. Fonseca, and I.A.A.C. Esteves, Biomass Valorization to Produce Porous Carbons: Applications in CO_2 Capture and Biogas Upgrading to Biomethane—A Mini-Review, *Front. Energy Res.*, 2021, **9**(March), p 1–6
43. R. Maniarasu, S.K. Rathore, and M. Sivalingam, *Simulation Study of Post-Combustion CO_2 Adsorption Using Adsorbent*. 2022, https://doi.org/10.4271/2022-28-0318
44. M. Jonnalagadda, R. Anjum, H. Burri, and S. Mutyala, Study of CO_2 Adsorption and Separation Using Modified Porous Carbon, *J. Chem. Res.*, 2021, **45**(1–2), p 194–200
45. M. Zhu, W. Cai, F. Verpoort, and J. Zhou, Preparation of Pineapple Waste-Derived Porouscarbons with Enhanced CO_2 Capture Performance by Hydrothermal Carbonation-Alkali Metal Oxalatesassisted Thermal Activation Process, *Chem. Eng. Res. Des.*, 2019, **146**, p 130–140
46. J. Wang, X. Yuan, S. Deng, X. Zeng, Z. Yu, S. Li, and K. Li, Waste Polyethylene Terephthalate (PET) Plastics-Derived Activated Carbon for CO_2 capture: A Route to a Closed Carbon Loop, *Green Chem.*, 2020, **22**(20), p 6836–6845
47. T. Cheng, Y. Jiang, Y. Zhang, and S. Liu, Prediction of Breakthrough Curves for Adsorption on Activated Carbon Fibers in a Fixed Bed, *Carbon N. Y.*, 2004, **42**(15), p 3081–3085
48. Q. Cen, M. Fang, J. Xu, and Z. Luo, Experimental Study of Breakthrough Adsorption on Activated Carbon for CO_2 Capture, *Adv. Mat. Res.*, 2012, **356–360**, p 1139–1144
49. Q. Zhu, Developments on CO_2-Utilization Technologies, *Clean Energy*, 2019, **3**(2), p 85–100

Publisher's Note Springer Nature remains neutral with regard to jurisdictional claims in published maps and institutional affiliations.

Springer Nature or its licensor (e.g. a society or other partner) holds exclusive rights to this article under a publishing agreement with the author(s) or other rightsholder(s); author self-archiving of the accepted manuscript version of this article is solely governed by the terms of such publishing agreement and applicable law.